Nondiffracting X Waves—Exact Solutions to Free-Space Scalar Wave Equation and Their Finite Aperture Realizations

Jian-yu Lu, *Member, IEEE*, and James F. Greenleaf, *Fellow, IEEE*

Abstract—**Novel families of generalized nondiffracting waves have been discovered. They are exact nondiffracting solutions of the isotropic/homogenous scalar wave equation and are a generalization of some of the previously known nondiffracting waves such as the plane wave, Durnin's beams, and the nondiffracting portion of the Axicon beam equation in addition to an infinity of new beams. One subset of the new nondiffracting waves have X-like shapes that are termed "X waves." These nondiffracting X waves can be almost exactly realized over a finite depth of field with finite apertures and by either broad band or band-limited radiators. With a 25 mm diameter planar radiator, a zeroth-order broadband X wave will have about 2.5 mm lateral and 0.17 mm axial −6-dB beam widths with a −6-dB depth of field of about 171 mm. The phase of the X waves changes smoothly with time across the aperture of the radiator, therefore, X waves can be realized with physical devices. A zeroth-order band-limited X wave was produced and measured in water by our 10 element, 50 mm diameter, 2.5 MHz PZT ceramic/polymer composite J_0 Bessel nondiffracting annular array transducer with −6-dB lateral and axial beam widths of about 4.7 mm and 0.65 mm, respectively, over a −6-dB depth of field of about 358 mm. Possible applications of X waves in acoustic imaging and electromagnetic energy transmission are discussed.**

I. Introduction

In 1983, J. N. Brittingham [1] discovered the first localized wave solution of the free-space scalar wave equation and called it a self focus wave mode. In 1985, another localized wave solution was discovered by R. W. Ziolkowski [2] who developed a procedure to construct new solutions [3] through the Laplace transform. These localized solutions were further studied by several investigators [4]–[9]. An acoustic device was constructed to realize Ziolkowski's Modified Power Spectrum pulse that is one of the solutions of the wave equation through the Laplace transform [10].

In 1987 J. Durnin discovered independently a new exact nondiffracting solution of the free-space scalar wave equation [11]. This solution was expressed in continuous wave form and was realized by optical experiments [12]. Durnin's beams were further studied in optics in a number of papers [13]–[19]. Hsu *et al.* [20] realized a J_0 Bessel beam with a narrow band PZT ceramic ultrasonic transducer of nonuniform poling. We made the first J_0 Bessel nondiffracting annular array transducer [21] with PZT ceramic/polymer composite and applied it to medical acoustic imaging and tissue characterization [22]–[25]. Campbell *et al.* had a similar idea to use an annular array to realize a J_0 Bessel nondiffracting beam and compared the J_0 Bessel beam to the Axicon [26].

In this paper, we report families of generalized nondiffracting solutions of the free-space scalar wave equation, and specifically, a subset of these nondiffracting solutions, which we term X waves (so-called X waves because of the appearance of the field distribution in a plane through the axis of the beam). The X waves are a frequency weighted Laplace transform of the nondiffracting portion of the Axicon beam equations [27]–[33] (in addition to the nondiffracting portion, the Axicon beam equation contains a factor that is proportional to $\sqrt{z}$ that will go to infinity as $z \to \infty$ [31]) and travel in free-space (or isotropic/homogeneous media) to infinite distance without spreading provided that they are produced by an infinite aperture.

Even with finite apertures, X waves have a large depth of field. (For example, with 25 mm diameter radiator, a zeroth-order broadband X wave will keep 2.5 mm and 0.17 mm −6-dB lateral and axial beam widths, respectively, and have a 171 mm depth of field that is about 68 times the −6-dB lateral beam width and 7 times the radiating diameter.) We have experimentally produced a zeroth-order band-limited X wave [34]. We used our 10 element, 50 mm diameter, 2.5 MHz PZT ceramic/polymer composite J_0 Bessel nondiffracting annular array transducer [21], [22]. The X wave had −6-dB lateral and axial beam widths of about 4.7 mm and 0.65 mm, respectively, over a −6-dB depth of field of about 358 mm.

In comparison with Ziolkowski's localized wave mode [2], [3], the peak pulse amplitude of the X wave is constant as it propagates to infinity because of its nondiffracting nature. Durnin's beams are nondiffracting at a single frequency but will diffract (or spread) in the temporal direction for multiple frequencies [22]. *X waves are multiple frequency waves but they are nondiffracting in both transverse and axial directions.*

Like the J_0 Bessel nondiffracting beam [21]–[25], X waves could be applied to acoustic imaging and tissue characterization. In addition, the space and time localization properties of X waves will allow particle-like energy transmission through large distances, as is the case with Ziolkowski's localized wave mode [7].

Manuscript received April 10, 1991; revised and accepted June 17, 1991. This work was supported in part by grant CA 43920 from the National Institutes of Health.

The authors are with the Biodynamics Research Unit, Department of Physiology and Biophysics, Mayo Clinic and Foundation, Rochester, MN 55905

IEEE Log Number 9103584.

In Section II, we first introduce the families of generalized nondiffracting waves and the nondiffracting X waves. Then, we provide two specific X wave examples. The production of X waves with realizable finite aperture radiators and finite bandwidths are reported in Section III. Finally, in Sections IV and V, we discuss further implications of these novel beams.

II. Theory of X Waves and Two Examples

We will show below three families of generalized nondiffracting solutions of the free space (or isotropic/homogeneous) scalar wave equation.

The free space scalar wave equation in cylindrical coordinates is given by

$$\left[\frac{1}{r}\frac{\partial}{\partial r}\left(r\frac{\partial}{\partial r}\right)+\frac{1}{r^2}\frac{\partial^2}{\partial\phi^2}+\frac{\partial^2}{\partial z^2}-\frac{1}{c^2}\frac{\partial^2}{\partial t^2}\right]\Phi=0. \quad (1)$$

where $r = \sqrt{x^2+y^2}$ represents radial coordinate, ϕ is azimuthal angle, z is axial axis, which is perpendicular to the plane defined by r and ϕ, t is time and Φ represents acoustic pressure or Hertz potential that is a function of r, ϕ, z, and t.

The three functions below are families of exact solutions of (1) (see the Appendix):

$$\Phi_\zeta(s)=\int_0^\infty T(k)\left[\frac{1}{2\pi}\int_{-\pi}^{\pi}A(\theta)f(s)d\theta\right]dk \quad (2)$$

$$\Phi_K(s)=\int_{-\pi}^{\pi}D(\zeta)\left[\frac{1}{2\pi}\int_{-\pi}^{\pi}A(\theta)f(s)d\theta\right]d\zeta \quad (3)$$

$$\Phi_L(r,\phi,z-ct)=\Phi_1(r,\phi)\Phi_2(z-ct) \quad (4)$$

where

$$s=\alpha_0(k,\zeta)r\cos(\phi-\theta)+b(k,\zeta)[z\pm c_1(k,\zeta)t] \quad (5)$$

and where

$$c_1(k,\zeta)=c\sqrt{1+[\alpha_0(k,\zeta)/b(k,\zeta)]^2} \quad (6)$$

where $T(k)$ is any complex function (well behaved) of k and could include the temporal frequency transfer function of a radiator system, $A(\theta)$ is any complex function (well behaved) of θ and represents a weighting function of the integration with respect to θ, $f(s)$ is any complex function (well behaved) of s, $D(\zeta)$ is any complex function (well behaved) of ζ and represents a weighting function of the integration with respect to ζ, which could be the Axicon angle ((11)), $\alpha_0(k,\zeta)$ is any complex function of k and ζ, $b(k,\zeta)$ is any complex function of k and ζ. The term c is constant in (1), k and ζ are variables that are independent of the spatial position, $\vec{r}=(r\cos\phi,\ r\sin\phi,\ z)$, and time, t, and $\Phi_2(z-ct)$ is any complex function of $z-ct$. $\Phi_1(r,\phi)$ is any solution of the following transverse Laplace equation (an example of $\Phi_1(r,\phi)$ is given in the Appendix):

$$\left[\frac{1}{r}\frac{\partial}{\partial r}\left(r\frac{\partial}{\partial r}\right)+\frac{1}{r^2}\frac{\partial^2}{\partial\phi^2}\right]\Phi_1(r,\phi)=0. \quad (7)$$

The exact solution of the free space scalar wave equation, Φ_L, represents a family of nondiffracting waves because if one travels with the wave at the speed, c, i.e., $z-ct$ =constant, both the lateral and axial complex field patterns, $\Phi_1(r,\phi)$ and $\Phi_2(z-ct)$, will be the same for all time, t, and distance, z.

If $c_1(k,\zeta)$ in (6) is real, "$\pm$" in (5) will represent backward and forward propagating waves, respectively. (In the following analysis, we consider only the forward propagating waves. All results will be the same for the backward propagating waves.) Furthermore, $\Phi_\zeta(s)$ and $\Phi_K(s)$ will also represent families of nondiffracting waves if $c_1(k,\zeta)$ is independent of k and ζ, respectively. These waves will travel to infinity at the speed of c_1 without diffracting or spreading in either the lateral or axial directions. This is different from Brittingham's focus wave mode [1], and Ziolkowski's localized wave [2] and modified power spectrum pulse [3] that contain both $z-ct$ and $z-c't$, or both $z-ct$ and $z+ct$ terms in their variables, where c and c' are different constants.

We find $\Phi_\zeta(s)$ is the most interesting solution. In the following, we will discuss $\Phi_\zeta(s)$ only. $\Phi_\zeta(s)$ is a generalized function that contains some of the nondiffracting solutions of the free space scalar wave equation known previously, such as, the plane wave, Durnin's nondiffracting beams, and the nondiffracting portion of the Axicon beam in addition to an infinity of new beams.

If $T(k)=\delta(k-k')$, where $\delta(k-k')$ is the Dirac–Delta function and $k'=\omega/c>0$ is a constant, $f(s)=e^s$, $\alpha_0(k,\zeta)=-i\alpha$, $b(k,\zeta)=i\beta=i\omega/c_1$, from (2) and (5), one obtains Durnin's nondiffracting beam [11]

$$\Phi_D(s)=\left[\frac{1}{2\pi}\int_{-\pi}^{\pi}A(\theta)e^{-i\alpha r\cos(\phi-\theta)}d\theta\right]e^{i(\beta z-\omega t)} \quad (8)$$

where

$$\beta=\sqrt{k'^2-\alpha^2} \quad (9)$$

where α is a constant and ω is angular frequency. If $A(\theta)=i^n e^{in\theta}$, we obtain the nth-order nondiffracting Bessel beams:

$$\Phi_{J_n}(s)=J_n(\alpha r)e^{i(\beta z-\omega t+n\phi)},\ (n=0,\ 1,\ 2,\ \cdots). \quad (10)$$

If $n=0$, one obtains the J_0 Bessel nondiffracting beam. From (8), it is seen that $c_1(k',\zeta)$ of the Durnin beams is equal to ω/β and is dependent upon k'. Therefore, if $T(k)$ in (2) is a complex function containing multiple frequencies, $\Phi_\zeta(s)$ will represent a dispersive wave and will diffract in the axial direction, z. If both n and α are zero, (10) represents the plane wave [11].

If in (2), we let $T(k)=\delta(k-k')$, $f(s)=e^s$, $A(\theta)=i^n e^\theta$, $\alpha_0(k,\zeta)=-ik\sin\zeta$, $b(k,\zeta)=ik\cos\zeta$, where $k'=\omega/c>0$ is a free parameter, and ζ represents the Axicon angle (we confine $0<\zeta<\pi/2$), we obtain the nth-order nondiffracting portion of the Axicon beam [31]:

$$\Phi_{An}(s)=J_n(k'r\sin\zeta)e^{i\left(k'z\cos\zeta-\omega t+n\phi\right)},\ (n=0,\ 1,\ 2,\ldots). \quad (11)$$

From (11), it is seen that $c_1(k',\zeta)=c/\cos\zeta$ is independent of k', which means that the waves constructed from $\Phi_{An}(s)$ by (2)

will have a constant speed c_1 for all frequency components and will be nondispersive. The X waves derived in the following are such waves that are nondiffracting or nonspreading in both lateral and axial directions.

We obtain the new X wave if in (2), we let $T(k) = B(k)e^{-a_0 k}$, $A(\theta) = i^n e^{in\theta}$, $\alpha_0(k,\zeta) = -ik\sin\zeta$, $b(k,\zeta) = ik\cos\zeta$, $f(s) = e^s$, obtaining

$$\Phi_{X_n} = e^{in\phi}\int_0^\infty B(k)J_n(kr\sin\zeta)e^{-k[a_0 - i(z\cos\zeta - ct)]}dk, \quad (n = 0,\ 1,\ 2, ...). \tag{12}$$

This is an integration of the nth-order nondiffracting portion ((11)) of the Axicon beam equation multiplied by $B(k)e^{-a_0 k}$, where $B(k)$ is any complex function (well behaved) of k and represents a transfer function of a practical radiator system, $k = \omega/c, a_0 > 0$ is a constant, and ζ is the Axicon angle [31]. From the previous discussion, it is seen that Φ_{X_n} is an exact nondiffracting solution of the free-space scalar-wave equation (1). Equation (12) shows that Φ_{X_n} is represented by a Laplace transform of the function, $B(k)J_n(kr\sin\zeta)$, and an azimuthal phase term, $e^{in\phi}$. Because the waves represented by Φ_{X_n} have an X-like shape in a plane through the axial axis of the waves, we call them nth-order X waves.

We finish this section with two new nondiffracting X wave examples. The first represents an X wave with broad bandwidth, while the second is a band-limited X wave.

Example 1: First, we describe an expression for an X wave produced by infinite aperture and broad bandwidth.

If, in (12), $B(k) = a_0$, we obtain from the Laplace transform tables [35]

$$a_0\int_0^\infty J_n(\alpha k)e^{-sk}dk = \frac{a_0\alpha^n}{\sqrt{\alpha^2 + s^2}\left(s + \sqrt{\alpha^2 + s^2}\right)^n} \tag{13}$$

giving an nth-order broadband X wave solution (exact solution of (1), see the Appendix):

$$\Phi_{XBB_n} = \frac{a_0(r\sin\zeta)^n e^{in\phi}}{\sqrt{M}\left(\tau + \sqrt{M}\right)^n} \quad , \quad (n = 0,\ 1,\ 2, ...) \tag{14}$$

where the subscript BB means "broadband," and

$$M = (r\sin\zeta)^2 + \tau^2 \tag{15}$$

and where

$$\tau = [a_0 - i(z\cos\zeta - ct)]. \tag{16}$$

For simplicity, we let n = 0, obtaining axially symmetric zeroth-order nondiffracting X wave:

$$\Phi_{XBB_0} = \frac{a_0}{\sqrt{(r\sin\zeta)^2 + [a_0 - i(zcos\zeta - ct)]^2}}. \tag{17}$$

The behavior of the analytic envelope of the real part of (17), $\mathrm{Re}[\Phi_{XBB_0}]$ is shown in the upper left panel of Fig. 1 or Fig. 2. The modulus of Φ_{XBB_0} in (17) can be obtained as shown in (18) (see bottom of page).

Now we discuss the lateral, axial, and X branch behaviors of this X wave. It is seen from (18) that for fixed ζ and a_0, at the plane $z = ct/\cos\zeta$, we have

$$|\ \Phi_{XBB_0}\ | = \frac{1}{\sqrt{1 + \left(\frac{\sin\zeta}{a_0}\right)^2 r^2}} \tag{19}$$

which represents the lateral pressure distribution of the X wave through the pulse center and has an asymptotic behavior proportional to $1/r$ when r is very large.

On the line $r = 0$, from (18), we obtain

$$|\ \Phi_{XBB_0}\ | = \frac{1}{\sqrt{1 + \left(\frac{\cos\zeta}{a_0}\right)^2\left(z - \frac{c}{\cos\zeta}t\right)^2}} \tag{20}$$

which is the pressure distribution of the X wave along the axial axis, z, and has an asymptotic behavior proportional to $1/|\ z - \frac{c}{cos\zeta}t\ |$ when $|\ z - \frac{c}{\cos\zeta}t\ |$ is very large.

The pressure distribution of the X wave along its two branches (see Figs. 1 and 2) can be obtained when

$$r = \frac{a_0}{\sin\zeta}\sqrt{\left(\frac{\cos\zeta}{a_0}\right)^2\left(z - \frac{c}{\cos\zeta}t\right)^2 - 1} \tag{21}$$

where

$$\frac{\cos\zeta}{a_0}\ |\ z - \frac{c}{\cos\zeta}t\ | \geq 1 \tag{22}$$

and from (18) we obtain

$$|\ \Phi_{XBB_0}\ | = \frac{1}{\sqrt{2\frac{\cos\zeta}{a_0}\ |\ z - \frac{c}{\cos\zeta}t\ |}} \tag{23}$$

which has an asymptotic behavior that is proportional to $1/\sqrt{|\ z - \frac{c}{cos\zeta}t\ |}$ when $|\ z - \frac{c}{\cos\zeta}t\ |$ is very large. This is the direction of slowest descent of the X wave amplitude from its center.

From (19), (20), and (23), it is seen that the smaller a_0 is, the faster the function $|\ \Phi_{XBB_0}\ |$ diminishes as r or $|\ z - \frac{c}{cos\zeta}t\ |$ increases. If $\sin\zeta$ is small, the diminution of $|\ \Phi_{XBB_0}\ |$ will be slow with respect to r and fast with respect to $|\ z - \frac{c}{cos\zeta}t\ |$. This means that if the X waves are applied to

$$|\ \Phi_{XBB_0}\ | = \frac{1}{\sqrt[4]{\left[1 + \left(\frac{\sin\zeta}{a_0}\right)^2 r^2 - \left(\frac{\cos\zeta}{a_0}\right)^2\left(z - \frac{c}{\cos\zeta}t\right)^2\right]^2 + 4\left(\frac{\cos\zeta}{a_0}\right)^2\left(z - \frac{c}{\cos\zeta}t\right)^2}}. \tag{18}$$

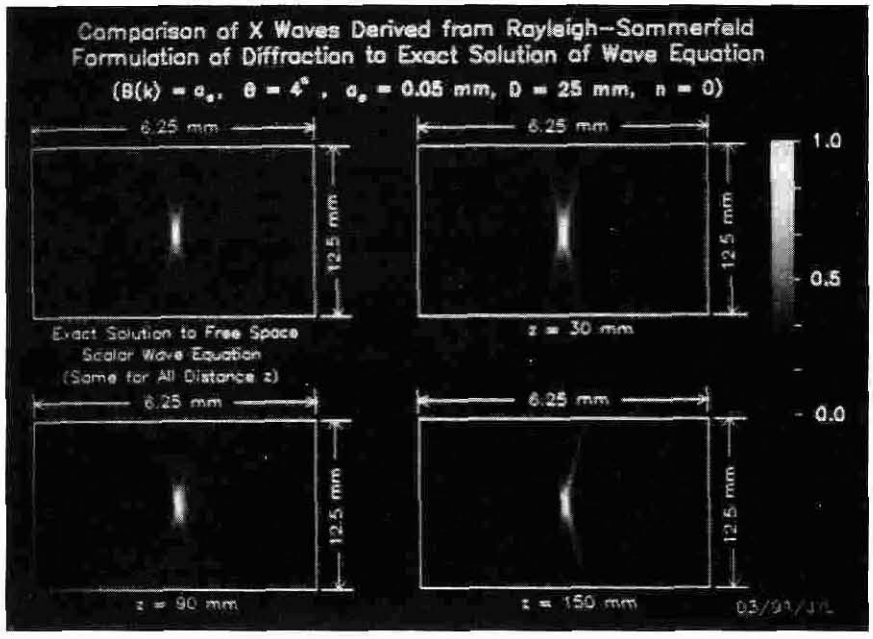

Fig. 1. Panel (a) represents the exact zeroth-order nondiffracting X wave solution of the free-space scalar wave equation. Panels (b), (c), and (d) are the appropriate zeroth-order nondiffracting X waves calculated from the Rayleigh–Sommerfeld diffraction integral with a 25-mm diameter planar radiator at distances z =30 mm, 90 mm, and 150 mm, respectively. The dimension of each panel is 12.5 mm × 6.25 mm. $B(k) = a_0$, $\zeta = 4°$ and $a_0 = 0.05$ mm.

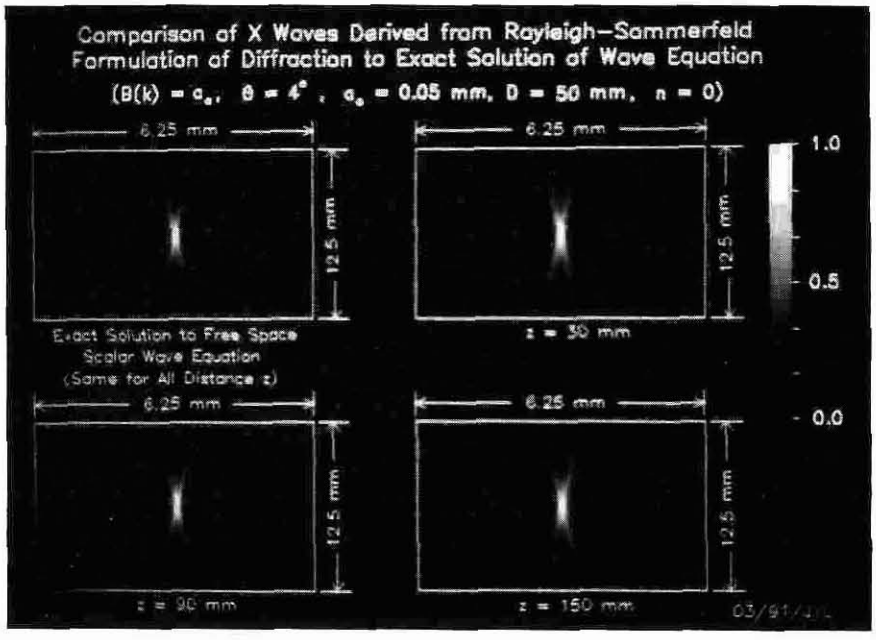

Fig. 2. Same format as Fig. 1, except that a 50 mm diameter planar radiator is used.

imaging, smaller a_0 will give better resolutions in both lateral and axial directions, while smaller $\sin\zeta$ will reduce the lateral resolution while increasing the axial resolution.

At the center of the zeroth-order X wave ($r = 0$, $z = ct/\cos\zeta$), $\Phi_{XBB_0} \equiv 1$ for all distance, z, and time, t (see (17)), which is unlike Ziolkowski's localized wave [2] and modified power spectrum pulses [3] that recover their pulse peak values periodically or aperiodically with distance, z.

Example 2: Because $B(k)$ in (12) is free, it may be chosen to achieve realizable bandwidth as shown in the following example. If $B(k)$ is a Blackman window function [36]:

$$B(k) = \begin{cases} a_0\left[0.42 - 0.5\cos\frac{\pi k}{k_0} + 0.08\cos\frac{2\pi k}{k_0}\right], & 0 \le k \le 2k_0 \\ 0, & \text{otherwise} \end{cases} \tag{24}$$

We can approximate the bandwidth of a real transducer. Although we cannot find an analytic expression for Φ_{X_n} from using (24) in (12) by directly looking up a Laplace transform table, we will describe in the Section III the resulting nondiffracting beam calculated for some finite apertures.

III. Realization of X Waves with Finite Aperture Radiators

The extension and therefore the aperture requirement of X waves in space is infinite (see (12)). But we show that nearly exact X waves can be realized with finite aperture radiators over large axial distance. To calculate X waves from the finite aperture radiators, a spectrum of X waves is used. Equation (12) can be rewritten as (25) (see bottom of page), which is an inverse Fourier transform of the function (spectrum of X waves)

$$\tilde{\Phi}_{X_n}\left(\vec{r},\frac{\omega}{c}\right) = \frac{2\pi}{c}e^{in\phi}B\left(\frac{\omega}{c}\right)J_n\left(\frac{\omega}{c}r\sin\zeta\right) \cdot H\left(\frac{\omega}{c}\right)e^{-\frac{\omega}{c}(a_0 - iz\cos\zeta)}, (n = 0, 1, 2, \ldots) \tag{26}$$

where

$$H\left(\frac{\omega}{c}\right) = \begin{cases} 1, & \omega \geq 0 \\ 0, & \omega < 0 \end{cases} \tag{27}$$

is the Heaviside step function [37].

At the plane $z = 0$, (26) becomes

$$\tilde{\Phi}_{X_n}\left(r,\phi,\frac{\omega}{c}\right) = B\left(\frac{\omega}{c}\right)E_n\left(r,\phi,\frac{\omega}{c}\right), (n = 0,1,2,\ldots) \tag{28}$$

where

$$E_n\left(r,\phi,\frac{\omega}{c}\right) = \frac{2\pi}{c}J_n\left(\frac{\omega}{c}r\sin\zeta\right) \cdot H\left(\frac{\omega}{c}\right)e^{-\frac{\omega a_0}{c}+in\phi}, \quad (n = 0, 1, 2, \ldots). \tag{29}$$

The spectrum in (28) is used to calculate X waves from radiators with finite aperture. If we assume that the radiator is circular and has a diameter of D, the Rayleigh–Sommerfeld formulation of diffraction by a plane screen [38] can be written as

$$\tilde{\Phi}_{R_n}(\vec{r},k) = \frac{1}{i\lambda}\int_0^{2\pi}d\phi'\int_0^{D/2}r'dr'\tilde{\Phi}_{X_n}(r',\phi',k)\frac{e^{ikr_{01}}}{r_{01}^2}z + \frac{1}{2\pi}\int_0^{2\pi}d\phi'\int_0^{D/2}r'dr'\tilde{\Phi}_{X_n}(r',\phi',k)\frac{e^{ikr_{01}}}{r_{01}^3}z, \quad (n = 0, 1, 2, \ldots) \tag{30}$$

and

$$\Phi_{R_n}(\vec{r},t) = \mathcal{F}^{-1}\left[\tilde{\Phi}_{R_n}\left(\vec{r},\frac{\omega}{c}\right)\right], \quad (n = 0, 1, 2, \ldots) \tag{31}$$

where λ is wavelength, r_{01} is the distance between the observation point, $\vec{r}$, and a point on the source plane (r', ϕ'), and $\mathcal{F}^{-1}$ represents the inverse Fourier transform. The first and second terms in (30) represent the contribution from high and low frequency components, respectively.

Because $B(\omega/c)$ in (28) is independent of r' and ϕ', (30) can be rewritten in another form

$$\tilde{\Phi}_{R_n}(\vec{r},k) = B(k)G_n(\vec{r},k), \quad (n = 0, 1, 2, \ldots) \tag{32}$$

where

$$G_n(\vec{r},k) = \frac{1}{i\lambda}\int_0^{2\pi}d\phi'\int_0^{D/2}r'dr'E_n(r',\phi',k)\frac{e^{ikr_{01}}}{r_{01}^2}z + \frac{1}{2\pi}\int_0^{2\pi}d\phi'\int_0^{D/2}r'dr'E_n(r',\phi',k)\frac{e^{ikr_{01}}}{r_{01}^3}z \quad (n = 0, 1, 2, \ldots) \tag{33}$$

and

$$\Phi_{R_n}(\vec{r},t) = \mathcal{F}^{-1}\left[B\left(\frac{\omega}{c}\right)G_n\left(\vec{r},\frac{\omega}{c}\right)\right] = \mathcal{F}^{-1}\left[B\left(\frac{\omega}{c}\right)\right] * \mathcal{F}^{-1}\left[G_n\left(\vec{r},\frac{\omega}{c}\right)\right] \tag{34}$$

where * denotes convolution on time, t, and $\mathcal{F}^{-1}[B(\omega/c)]$ can be taken as an impulse response of the radiator.

We now describe an example of an X wave produced by a finite aperture. Let $B(k) = a_0$, $\zeta = 4^O$, ($\sin 4^O \approx 0.0698$, $\cos 4^O \approx 0.998$), $a_0 = 0.05$ mm, $n = 0$, and $c = 1.5$ mm/μs (speed of sound in water). The analytic envelope of the real part of Φ_{R_0}, $Re[\Phi_{R_0}]$, calculated from (33) and (34) is given in Fig. 1 and Fig. 2, when the diameter of the radiator, D, is 25 mm and 50 mm, respectively. The X waves are shown at $z = 30$mm, 90 mm, and 150 mm, respectively. These X waves compared well to the analytic envelope of the real part of the exact nondiffracting X wave solution, $Re[\Phi_{XBB_0}]$, where Φ_{XBB_0} is given by (17) (see upper-left panel of Fig. 1 or 2).

Fig. 3 shows beam plots of the X waves in Figs. 1 and 2. Figs. 3(a1), 3(a2), and 3(a3) represent the lateral beam plots of the X waves produced at the axial distances z =30 mm, 90 mm, and 150 mm, respectively, through the center of the pulses. The full, dotted, and dashed lines represent the beam plots of the X waves produced by a 25 mm diameter radiator, 50 mm diameter radiator, and the exact nondiffracting X wave solution of the free-space scalar wave equation (real part of (17)), respectively. Fig. 3(a4) represents the peak of the X waves along the axial distance, z, from 6 mm to 400 mm. The –6-dB depths of field of the X waves are about 171 mm and 348 mm when the radiator has diameters of 25 mm and 50 mm, respectively. The −6-dB lateral beam width throughout the depth of field is about 2.5 mm.

$$\Phi_{X_n} = \frac{1}{2\pi}\int_{-\infty}^{\infty}\left[\frac{2\pi}{c}e^{in\phi}B\left(\frac{\omega}{c}\right)J_n\left(\frac{\omega}{c}r\sin\zeta\right)H\left(\frac{\omega}{c}\right)e^{-\frac{\omega}{c}(a_0 - iz\cos\zeta)}\right]e^{-i\omega t}d\omega, \ (n = 0, 1, 2, \ldots), \tag{25}$$

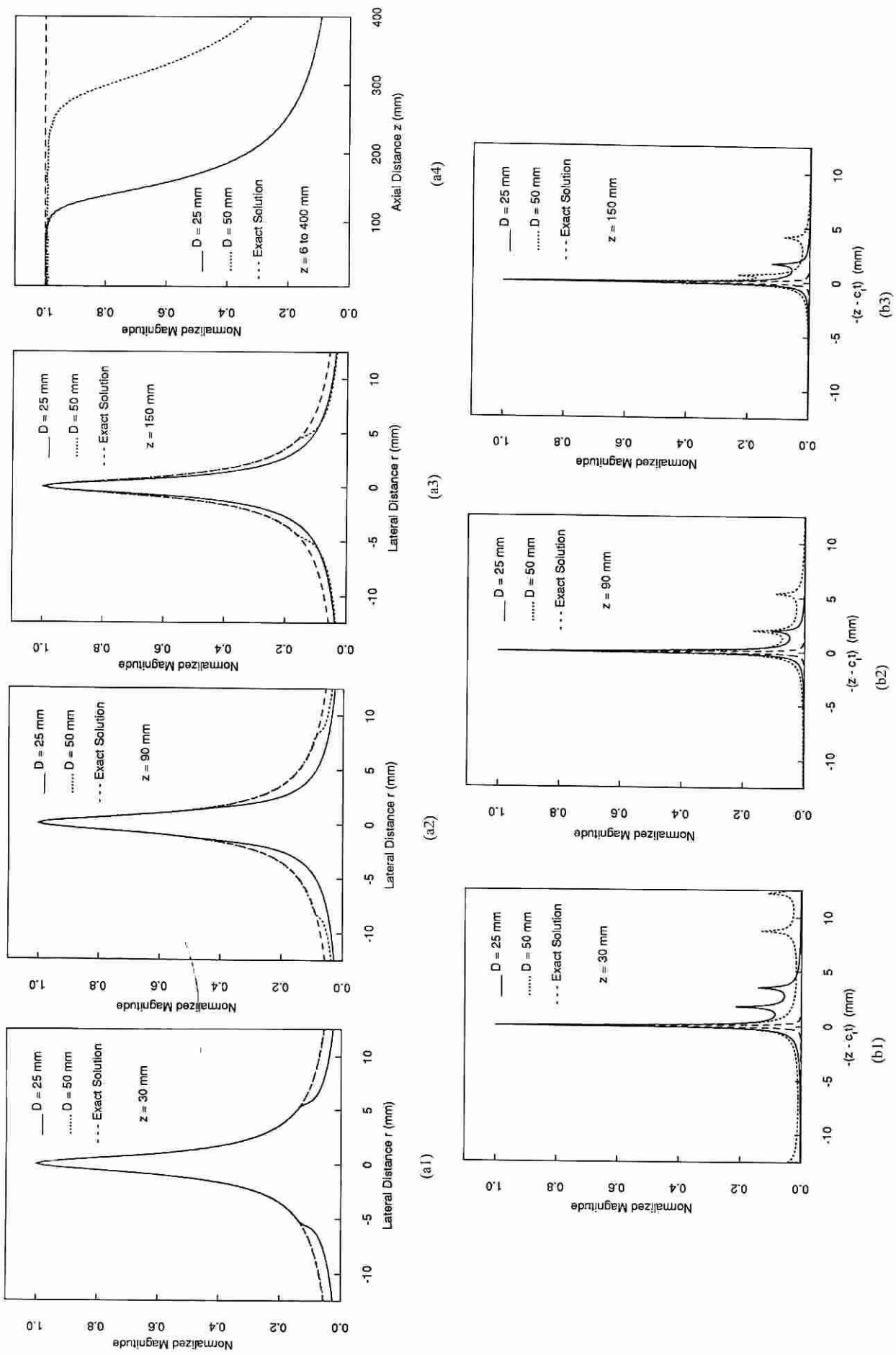

Fig. 3. (a) Lateral (except (a4)) and (b) axial beam plots of the nondiffracting X waves in Figs. 1 and 2 at distances (1) $z = 30$ mm, (2) $z = 90$ mm, and (3) $z = 150$ mm. Full lines, dotted lines, and dashed lines represent the beam plots of the X waves produced by a radiator of diameter of 25 mm, 50 mm, and by the exact solution of the free-space scalar wave equation, respectively. (a4) plots of the peak value of the X waves along the axial axis from $z = 6$ mm to 400 mm. $z - c_1 t$ represents the axial distance away from the X wave pulse center. $c_1 = c/\cos\zeta$.

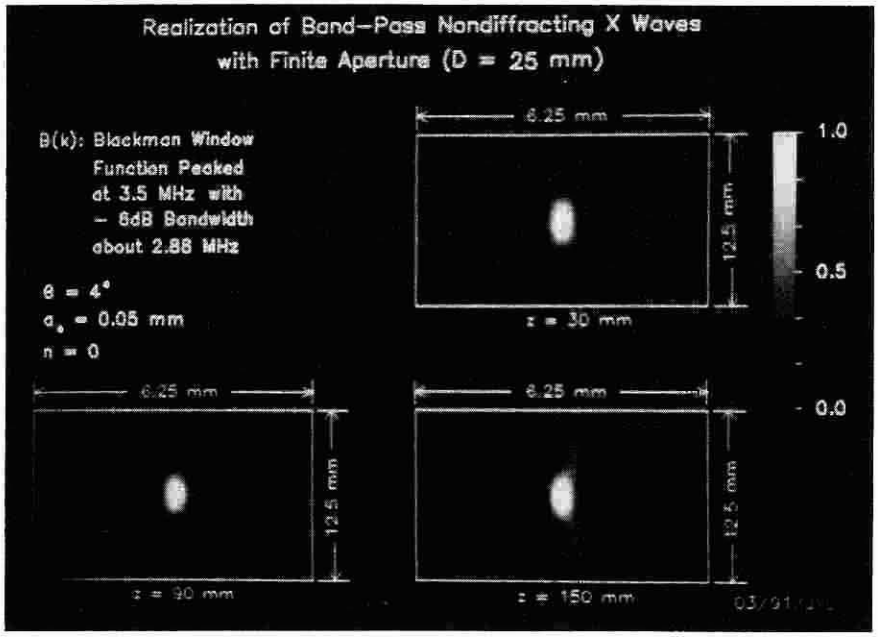

Fig. 4. Rayleigh–Sommerfeld calculation of the zeroth-order nondiffracting X waves produced by a 25 mm diameter, band-limited planar radiator at distances z =30 mm, 90 mm, and 150 mm. The radiator transfer function $B(k)$ is a Blackman window function peaked at 3.5 MHz with a −6-dB bandwidth about 2.88 MHz. The dimension of each panel is 12.5 mm × 6.25 mm. ζ = 4° and a_0 =0.05 mm.

Figs. 3(b1) to 3(b3) are axial beam plots of the X waves with respect to $c_1t - z$ and correspond to Figs. 3(a1) to 3(a3), respectively. ($c_1 = c/\cos\zeta$. For $\zeta = 4^o$, $c_1 \approx 1.002c$.) The edge waves produced by the sharp truncation of the pressure at the edge of the radiator are clearly seen. These edge waves can be overcome by using proper aperture apodization techniques [39] and will be discussed in the next section. The −6-dB axial beam width obtained from Fig. 3(b) is about 0.17 mm.

The depth of field and the lateral and axial beam widths of the zeroth-order broadband X wave produced by a radiator of diameter D can be determined analytically in the following. For any given angular frequency, ω_0, (30) represents a continuous field of an aperture shaded by a J_0 Bessel function

$$S(\omega_0)J_0(\alpha_0 r) \tag{35}$$

where

$$S(\omega_0) = \frac{2\pi}{c}B\Big(\frac{\omega_0}{c}\Big)H\Big(\frac{\omega_0}{c}\Big)e^{-\frac{\omega_0 a_0}{c}} \tag{36}$$

and

$$\alpha_0 = \frac{\omega_0}{c}\sin\zeta. \tag{37}$$

The depth of field of this J_0 Bessel beam is determined by [11]

$$Z_{max} = \frac{D}{2}\sqrt{\left(\frac{\omega_0}{\alpha_0 c}\right)^2 - 1}. \tag{38}$$

Substituting (37) into (38), we obtain

$$Z_{max} = \frac{D}{2}\cot\zeta \tag{39}$$

which is independent of frequency ω_0! If ζ= 4^o and D = 25mm, we obtain, from (39), $z_{\max}$=178.8 mm, which is very close to what we obtained from Fig. 3(a)(4) (171 mm).

The −6-dB lateral beam width of the X waves can be calculated from (19), which is

$$2r = \frac{2\sqrt{3}a_0}{\sin\zeta} \tag{40}$$

and the −6-dB axial beam width is obtained from (20)

$$2\mid z - \frac{c}{\cos\zeta}t\mid = \frac{2\sqrt{3}a_0}{\cos\zeta}. \tag{41}$$

When a_0 = 0.05 mm and ζ = 4°, the calculated −6-dB lateral and axial beam widths are about 2.5 mm and 0.17 mm, respectively, which are the same as we measured from Fig. 3.

Figs. 4 and 5 are the analytic envelope of a zeroth-order band-limited nondiffracting X wave produced by a radiator of diameter of 25 mm and 50 mm, respectively, when $B(k)$ is chosen as a Blackman window function (see (24)). The parameter k_0 in (24) for these figures is given by

$$k_0 = \frac{2\pi f_0}{c} \tag{42}$$

where c =1.5 mm/μs, f_0 =3.5 MHz, and the −6-dB bandwidth of the Blackman window function is about 2.88 MHz. The X waves in Figs. 4 and 5 are a band-limited version of those in Figs. 1 and 2. They are the finite aperture realization of the convolution of function $\mathcal{F}^{-1}[B(\omega/c)]/a_0$ with (14) when $n = 0$, that is

$$\Phi_{XBL_n} = \frac{1}{a_0}\mathcal{F}^{-1}\Big[B\Big(\frac{\omega}{c}\Big)\Big] * \Phi_{XBB_n}, \quad (n = 0, 1, 2, \ldots) \tag{43}$$

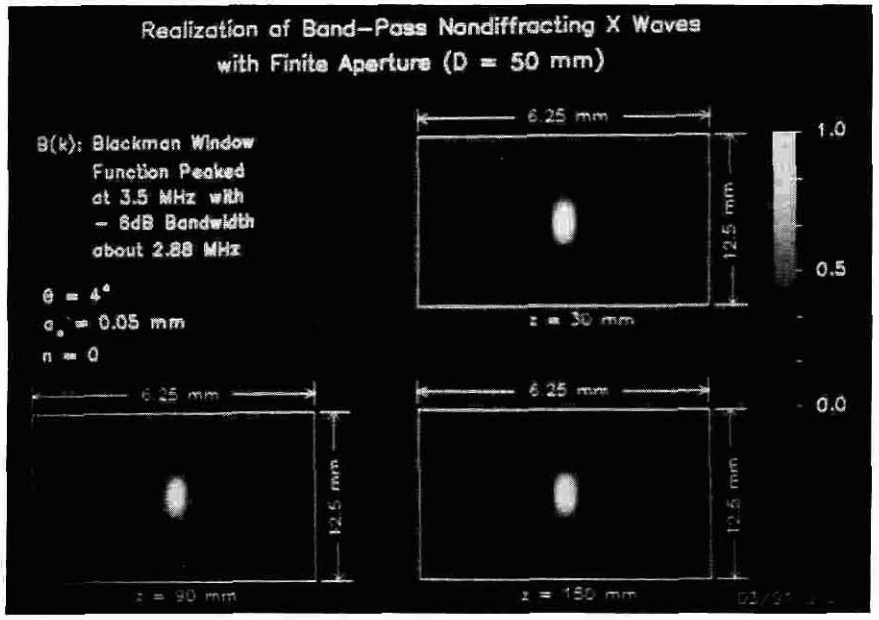

Fig. 5. Same format as Fig. 4, except that a 50 mm diameter planar radiator is used.

with $n = 0$, where $B(\omega/c)$ $(\omega \geq 0)$ can be any complex function that makes the integral in (25) converge, "*" denotes the convolution with respect to time, t, and the subscript BL represents "band-limited."

The three panels in Figs. 4 and 5 represent band-limited X waves at distance z =30 mm, 90 mm, and 150 mm, respectively. The parameters ζ and a_0 are the same as those in Figs. 1 and 2, which are 4° and 0.05 mm, respectively. From Figs. 4 and 5, it is seen that the band-limited X waves have lower field amplitude in the X branches than the wideband X waves in Figs. 1 and 2.

Fig. 6 is the same as Fig. 3, except that it represents the lateral and axial beam plots of the band-limited X waves in Figs. 4 and 5. The −6-dB lateral and axial beam widths of the band-limited X waves obtained from Fig. 6 are about 3.2 mm and 0.5 mm, respectively, at all three distances (z =30 mm, 90 mm, and 150 mm). Therefore, these band-limited X waves are also nondiffracting waves. Their −6-dB maximum nondiffracting distances derived from Fig. 6 are 173 mm and 351 mm, when the diameters of the radiators are 25 mm and 50 mm, respectively. The depths of field of the band-limited X waves are almost the same as those of the broad band nondiffracting X waves obtained from Fig. 3 and are very close to those calculated from (39).

IV. Discussion

A. Other Nondiffracting Solutions

From (43), it is seen that an infinity of nondiffracting X wave solutions with lower field amplitude in their X branches can be obtained by choosing different complex functions $B(k)$. In practice, $B(k)$ can be a transfer function of physical devices, such as acoustical transducers, electromagnetic antennas or other wave sources and their associated electronics. The Rayleigh–Sommerfeld formulation of diffraction [38] can be used to simulate the resulting beams.

Besides the X waves, there are many other families of nondiffracting waves that are also exact solutions of the free-space scalar wave equation (see (3) and (4) and the Appendix).

B. Resolution, Depth of Field, and Sidelobes of X Waves

From (18), it is seen that as a_o decreases, the X waves diminish faster with both r and $| z - (c/\cos\zeta t) |$, and hence they have higher lateral and axial resolution. This requires that the radiator system has a broader bandwidth because the term $\exp\{-a_0\omega/c\}$ in (26) will diminish slower for smaller a_0. For larger values of $\sin\zeta$, the lateral resolution will be increased while the axial resolution is decreased. The −6-dB lateral and axial beam widths of the zeroth-order broadband nondiffracting X waves ((17)) are determined by (40) and (41), respectively.

For finite aperture, the X waves are nondiffracting only within the depth of field. The depth of field of finite aperture nondiffracting X waves is related only to the size of the radiator and the Axicon angle ζ ((39)). Bigger values of $\sin\zeta$ will increase the lateral resolution ((40)) but reduce the depth of field. This trade-off is similar to that of conventional focused beams. For band-limited nondiffracting X waves, the lateral and axial beam widths are increased from those of the broadband X waves, but the depth of field is about the same.

The X waves have no or lower sidelobes in the $(z - c_1 t)$ plane than the J_0 Bessel nondiffracting beam [21], see Figs. 3 and 6. They do have energy along the branches of the X that becomes smaller as the radius r increases (see Figs. 1, 2, 4, and 5). It is fortuitous that the realizable band-limited X waves present lower field amplitude in their X branches than the broadband X waves (Figs. 4 and 5). In acoustical imaging, the effect of energy in the X branches could be suppressed dramatically by combining X wave transmit with dynamic

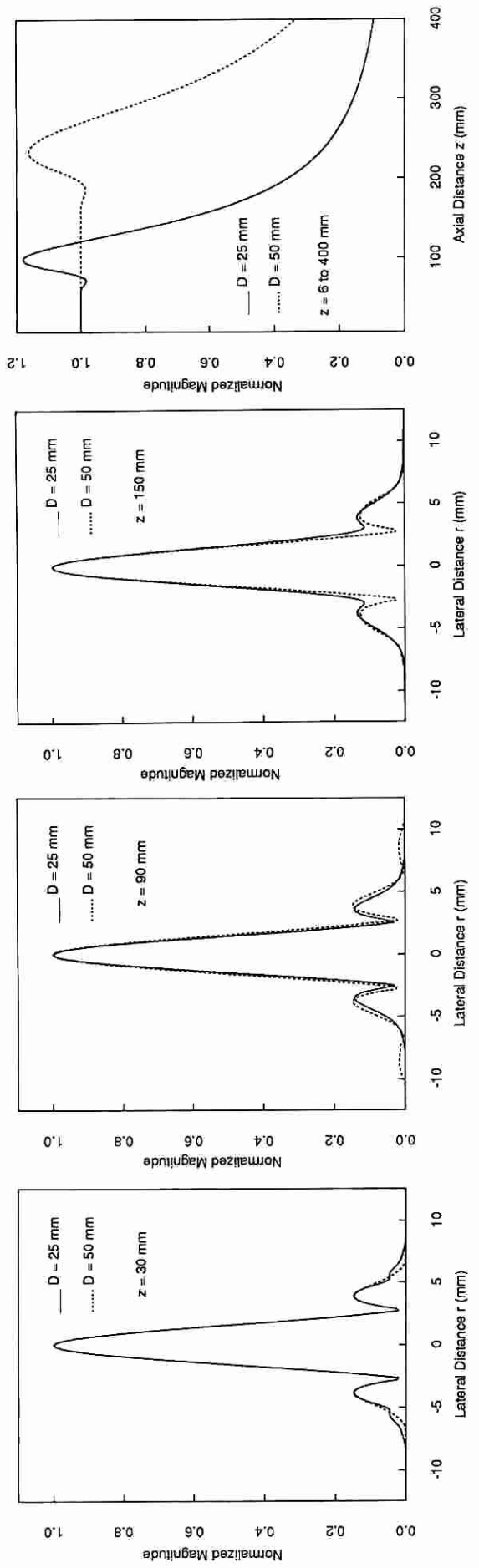

Fig. 6. (a) Lateral (except (a4)) and (b) axial beam plots of the band-limited nondiffracting X waves in Figs. 4 and 5 at distances (1) $z = 30$ mm, (2) $z = 90$ mm, and (3) $z = 150$ mm. Full and dotted lines represent the beam plots of the X waves produced by a radiator of diameter of 25 mm and 50 mm, respectively. (a4) Peak value of the X waves along the axial axis from $z = 6$ mm to 400 mm. $z - c_1 t$ represents the axial distance away from the X wave pulse center. $c_1 = c/\cos\zeta$.

spherical focused receiving as was proposed for the J_0 Bessel nondiffracting beam [25].

C. Edge Waves and Propagation Speed of the X Waves

It is seen from Figs. 3(b) and 6(b) that there is some energy in the waves produced by the edge of the aperture because of sharp truncation of the pressure at the edge of the radiators. These edge waves can be reduced by apodization techniques [39] that use window functions to apodize the edge of the aperture. (The results in Figs. 1 to 6 are obtained with a rectangular window aperture weighting.)

Fig. 7 shows reduction of the edge waves with aperture apodization. Figs. 7(a) (except panel (4)) and 7(b) show the lateral and axial beam plots, respectively, of band-limited X waves produced by a 25-mm-diameter radiator. The full and dotted lines represent the beam plots before and after the aperture apodization, respectively. The apodization function is given by (44) (see bottom of page), where $r_1 = 3D/8$, D is the diameter of the radiator, and r is the lateral distance from the center of the radiator. Panels (1), (2), and (3) in both Figs. 7(a) and 7(b) represent the beam plots at distance z =30 mm, 90 mm, and 150 mm, respectively. Fig. 7(a4) plots the peak value of the X wave along the axial axis from z =6 mm to 400 mm. The edge waves are reduced around 10 dB within the depth of field by the aperture apodization. The depth of field of the X wave is reduced from 173 mm to about 147 mm after the aperture apodization because of the reduced effective size of the aperture.

From (17), it is seen that the X waves travel with a speed faster than sound or light speed, c (superluminal). For example, if $\zeta = 4^0$, the X waves will travel about 0.2% faster than c. This is also the case of Durnin's J_0 Bessel beam. From (10), for $n = 0$, we obtain

$$\Phi_{J_0}(r, z - c_1 t) = J_0(\alpha r) e^{i\beta(z - c_1 t)}, \tag{45}$$

where $c_1 = \omega/\beta$ and $\beta = \sqrt{k^2 - \alpha^2} < k$. Therefore, $c = \omega/k < c_1$.

This is explained in the following: For large radius, r, on the surface of a radiator, the wavefront of the X wave is advanced. It is these wave fronts that construct the X wave at large distances as the influence of the wave fronts from the center of the radiator dies out. The wave energy radiated from each side of the radiator travels at the speed of sound, c, but the intersection, or peak, of these waves travels greater than the speed of sound.

D. Total Energy, Energy Density and Causality

Like the plane wave and Durnin's beam, the total energy of an X wave is infinite. But, the energy density of all these waves is finite. Approximate X waves are realizable with finite apertures and with finite energy over a deep depth of field.

From (17), it is seen that at a given distance z, the X waves extend from $t > -\infty$ to $t < \infty$. Therefore, they are not causal, but the X waves produced by fininte aperture diminish very fast as $|t| \to \infty$. If we ignore the X waves for $|t| > t_0$, where $|\Phi_{X_n}(\vec{r}, t_0)| << 1$, these modified X waves can be treated as causal waves. Similarly, Ziolkowski's localized wave [2], and modified power spectrum wave [3] suffer from the problem of causality, but they are closely approximated with finite aperture by using this same causal approximation [10].

We do not worry about the superluminal solutions, noncausal solutions, infinite total energy or infinite apertures as long as the pressure distributions over an aperture are sufficiently well behaved that they can be physically realized and truncated in time and space and still produce a wave of practical usefulness. Theoretical X waves are superluminal, noncausal, and have infinite total energy and apertures, but they can be truncated to produce practical waves. One example was given in reference [34], where a zeroth-order X wave was physically realized over a deep depth of field in an experiment using an acoustic annular array transducer [21], [22].

E. Application of X Waves to Acoustic Imaging and Electromagnetic Energy Transmission

The real part of (17), $\mathrm{Re}[\Phi_{XBB_0}]$, has a smooth phase change over time, t, across the transverse direction, r. This makes it possible to realize X waves with physical devices. Therefore, a broadband acoustic transducer could be used to produce X waves in Figs. 1 to 3, while a band-limited transducer could generate those in Figs. 4 to 6. The electrodes of an acoustic broadband PZT ceramic/polymer composite transducer can be cut into annular elements [21] and each element driven with a proper waveform depending upon its radial position. Annular array transducers can be used for both X wave transmitting and conventional dynamically spherical focused receiving [34]. The low sidelobes of a Gaussian shaded receiving would suppress the off-center X wave energy and produce high resolution, high frame rate, and large depth of field acoustic images.

The X wave solution to the free-space scalar wave equation can also be applied to electromagnetic energy transmission for private communication and military applications [7]. (Nondiffracting electromagnetic X waves are discussed in detail in [40].)

V. Conclusion

We have developed a new family of nondiffracting waves that provides a novel way to produce focused beams without lenses. They are realizable with finite apertures and with broadband and band-limited planar radiators with deep depth of field. The energy on the X branches of the X waves could be suppressed dramatically in imaging by combining the X

$$w(r) = \begin{cases} 1.0 \quad , \quad 0 \le r < r_1 \\ 0.42 - 0.5\cos\frac{2\pi\left(r + \frac{D}{2} - 2r_1\right)}{D - 2r_1} + 0.08\cos\frac{4\pi\left(r + \frac{D}{2} - 2r_1\right)}{D - 2r_1}, \quad r_1 \le r \le \frac{D}{2} \end{cases} \tag{44}$$

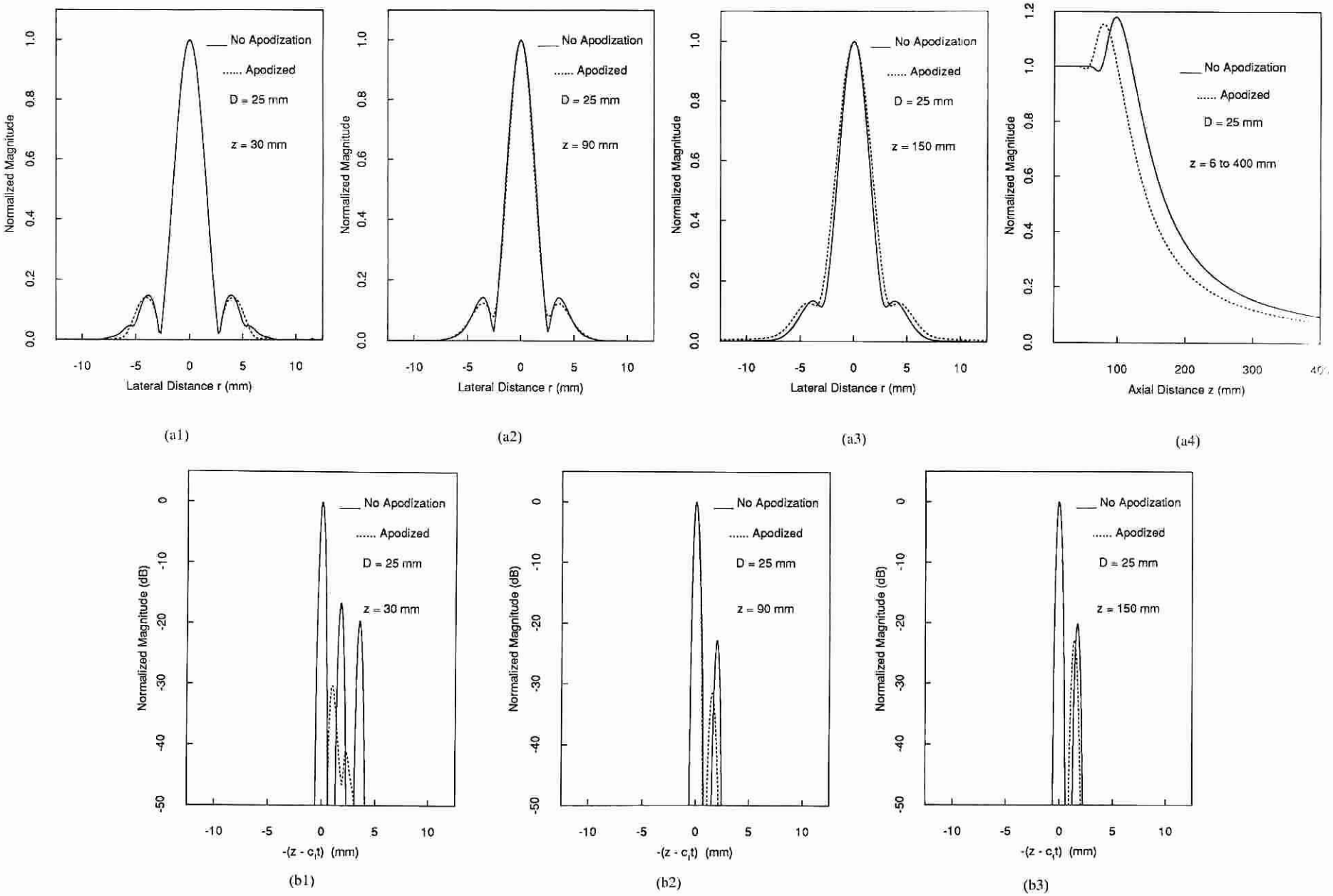

Fig. 7. Edge wave reduction with an aperture apodization function ((44)). (a) lateral (except (a4)) and (b) axial beam plots of the band-limited zeroth-order nondiffracting X waves produced at distance (1) $z = 30$ mm, (2) $z = 90$ mm, and (3) $z = 150$ mm. (a4) represents the peak of the X waves along the axial axis from $z = 6$ mm to 400 mm ($c_1 = c/\cos\zeta$). Full and dotted lines represent the beam plots before and after the aperture apodization, respectively. The diameter of the transducer is 25 mm. The edge waves were reduced around 10 dB within the depth of field (147 mm for apodized aperture).

waves with a conventional dynamically spherical focused receiving system to produce high contrast images [22]. Characterization of tissue properties could be simplified because of the absence of diffraction in X waves. In addition, the space and time localization properties of X waves will allow particle-like energy transmission through large distances, as is the case of Ziolkowski's localized wave mode [7].

APPENDIX

Theorem: Functions $\Phi_\zeta(s)$, $\Phi_K(s)$, and $\Phi_L(s)$ are exact solutions of the free-space scalar-wave equation (1).

Proof: The functions $\Phi_\zeta(s)$ and $\Phi_K(s)$ are linear summations of function $f(s)$ over free parameters k and ζ, respectively, see (2) and (3). Therefore, if we can prove $f(s)$ is an exact solution of (1), $\Phi_\zeta(s)$ and $\Phi_K(s)$ will also be exact solutions. (For example, one can directly prove that (14) is an exact solution of the free-space scalar wave (1). Using the expression of s in (5), we obtain

$$r\frac{\partial f}{\partial r} = r\frac{\partial f}{\partial s}\alpha_0(k,\zeta)\cos(\phi-\theta) \tag{46}$$

$$\frac{1}{r}\frac{\partial}{\partial r}\left(r\frac{\partial f}{\partial r}\right) = \frac{1}{r}\left[\frac{\partial f}{\partial s}\alpha_0(k,\zeta)\cos(\phi-\theta) + r\frac{\partial^2 f}{\partial s^2}\alpha_0^2(k,\zeta)\cos^2(\phi-\theta)\right] \tag{47}$$

$$\frac{\partial f}{\partial \phi} = \frac{\partial f}{\partial s}[-\alpha_0(k,\zeta)r\sin(\phi-\theta)] \tag{48}$$

$$\frac{1}{r^2}\frac{\partial^2 f}{\partial \phi^2} = \frac{1}{r^2}\frac{\partial^2 f}{\partial s^2}\alpha_0^2(k,\zeta)r^2\sin^2(\phi-\theta) + \frac{1}{r^2}\frac{\partial f}{\partial s}[-\alpha_0(k,\zeta)r\cos(\phi-\theta)] \tag{49}$$

$$\left[\frac{1}{r}\frac{\partial}{\partial r}\left(r\frac{\partial}{\partial r}\right) + \frac{1}{r^2}\frac{\partial^2}{\partial \phi^2}\right]f = \frac{\partial^2 f}{\partial s^2}\alpha_0^2(k,\zeta) \tag{50}$$

$$\frac{\partial^2 f}{\partial z^2} = \frac{\partial^2 f}{\partial s^2}b^2(k,\zeta) \tag{51}$$

$$-\frac{1}{c^2}\frac{\partial^2 f}{\partial t^2} = -\frac{1}{c^2}\frac{\partial^2 f}{\partial s^2}b^2(k,\zeta)c_1^2(k,\zeta) \tag{52}$$

$$\left[\frac{1}{r}\frac{\partial}{\partial r}\left(r\frac{\partial}{\partial r}\right) + \frac{1}{r^2}\frac{\partial^2}{\partial \phi^2} + \frac{\partial^2}{\partial z^2} - \frac{1}{c^2}\frac{\partial^2}{\partial t^2}\right]f = \frac{\partial^2 f}{\partial s^2}\left[\alpha_0^2(k,\zeta) + b^2(k,\zeta) - \frac{1}{c^2}b^2(k,\zeta)c_1^2(k,\zeta)\right]. \tag{53}$$

Using (6), the right-hand side of (53) is zero. Therefore, $\Phi_\zeta(s)$ and $\Phi_K(s)$ are exact solutions of the free-space scalar wave equation (1).

Now we prove $\Phi_L(s)$ in (4) is also an exact solution of (1):

$$\left[\frac{1}{r}\frac{\partial}{\partial r}\left(r\frac{\partial}{\partial r}\right) + \frac{1}{r^2}\frac{\partial^2}{\partial \phi^2} + \frac{\partial^2}{\partial z^2} - \frac{1}{c^2}\frac{\partial^2}{\partial t^2}\right]\Phi_L = \left\{\left[\frac{1}{r}\frac{\partial}{\partial r}\left(r\frac{\partial}{\partial r}\right) + \frac{1}{r^2}\frac{\partial^2}{\partial \phi^2}\right]\Phi_1(r,\phi)\right\}\Phi_2(z-ct). \tag{54}$$

Because $\Phi_1(r,\phi)$ is an exact solution of the transverse Laplace equation ((7)), the right-hand side of (54) is zero. This proves that Φ_L is an exact solution of the free-space scalar wave equation (1).

For example, if we choose $\Phi_2(z-ct)$ as a Gaussian pulse

$$\Phi_2(z-ct) = e^{-(z-ct)^2/\sigma^2}, \tag{55}$$

and $\Phi_1(r,\phi)$ as Poisson's formula [41, p. 373]

$$\Phi_1(r,\phi) = \frac{1}{2\pi}\int_{-\pi}^{\pi} f(\theta)\frac{a^2-r^2}{a^2-2ra\cos(\theta-\phi)+r^2}d\theta, \tag{56}$$

where

$$\Phi_1(r,\phi)|_{r=a} = f(\phi), \tag{57}$$

and $f(\phi)$ is any function (well-behaved) of ϕ, and σ and a are constants, the Gaussian pulse with a transverse field pattern $\Phi_1(r,\phi)$ will travel to infinity at the speed of sound or light without any change of pulse shape.

The transverse field ((56)) has the following properties:

$$\begin{cases} \lim_{r\to\infty}\Phi_1(r,\phi) = \lim_{r\to 0}\Phi_1(r,\phi) = \frac{1}{2\pi}\int_{-\pi}^{\pi} f(\theta)d\theta \\ If\ r_1/a = a/r_2, \qquad \Phi_1(r_1,\phi) = \Phi_1(r_2,\phi). \end{cases} \tag{58}$$

This means that if $\lim_{r\to\infty}\Phi_1(r,\phi) = 0$, then $\Phi_1(0,\phi) = 0$.

ACKNOWLEDGMENT

The authors appreciated the secretarial assistance of Elaine C. Quarve and the graphic assistance of Christine A. Welch.

REFERENCES

[1] J. B. Brittingham, "Focus wave modes in homogeneous Maxwell's equations: transverse electric mode," *J. Appl. Phys.*, vol 54, no. 3, pp. 1179–1189, 1983.

[2] R. W. Ziolkowski, "Exact solutions of the wave equation with complex source locations," *J. Math. Phys.*, vol. 26, no. 4, pp. 861–863, Apr., 1985.

[3] R. W. Ziolkowski, D. K. Lewis, and B. D. Cook, "Evidence of localized wave transmission," *Phys. Rev. Lett.*, vol. 62, no. 2, pp. 147–150, Jan. 9, 1989.

[4] A. M. Shaarawi, I. M. Besieris, and R. W. Ziolkowski, "Localized energy pulse train launched from an open, semi-infinite, circular waveguide," *J. Appl. Phys.*, vol. 65, no. 2, pp. 805–813, 1989.

[5] I. M. Besieris, A. M. Shaarawi, and R. W. Ziolkowski, "A bidirectional traveling plane wave representation of exact solutions of the scalar wave equation," *J. Math. Phys.*, vol. 30, no. 6, pp. 1254–1269, 1989.

[6] E. Heyman, B. Z. Steinberg, and L. B. Felsen, "Spectral analysis of focus wave modes," *J. Opt. Soc. Am. A* , vol. 4, no. 11, pp. 2081–2091, Nov., 1987.

[7] R. W. Ziolkowski, "Localized transmission of electromagnetic energy," *Phys. Rev. A.*, vol. 39, no. 4, pp. 2005–2033, Feb. 15, 1989.

[8] J. V. Candy, R. W. Ziolkowski, and D. K. Lewis, "Transient waves: reconstruction and processing," *J. Acoust. Soc. Am.*, vol. 88, no. 5, pp. 2248–2258, Nov., 1990.

[9] ——, "Transient wave estimation: a multichannel deconvolution application," *J. Acoust. Soc. Am.*, vol. 88, no. 5, pp. 2235–2247, Nov., 1990.

[10] R. W. Ziolkowski and D. K. Lewis, "Verification of the localized wave transmission effect," *J. Appl. Phys.*, vol. 68, no. 12, pp. 6083–6086, Dec. 15, 1990.
[11] J. Durnin, "Exact solutions for nondiffracting beams—I: The scalar theory," *J. Opt. Soc.*, vol. 4, no. 4, pp. 651–654, 1987.
[12] J. Durnin, J. J. Miceli, Jr., and J. H. Eberly, "Diffraction-free beams," *Phys. Rev. Lett.*, vol. 58, no. 15, pp. 1499–1501, Apr. 13, 1987.
[13] J. Durnin, J. J. Miceli, Jr., and J. H. Eberly, "Experiments with nondiffracting needle beams," Optical Soc. Amer., Washington, DC, available from IEEE Service Center (cat. no. 87CH2391–1), Piscataway, NJ, p. 208, 1987.
[14] G. Indebetow, "Nondiffracting optical fields: Some remarks on their analysis and synthesis," *J. Opt. Soc. Am. A*, vol. 6, no. 1, pp. 150–152, Jan., 1989.
[15] F. Gori, G. Guattari, and C. Padovani, "Model expansion for J_0-correlated Schell-model sources," *Optics Commun.*, vol. 64, no. 4, pp. 311–316, Nov. 15, 1987.
[16] K. Uehara and H. Kikuchi, "Generation of near diffraction-free laser beams," *Appl. Physics B*, vol. 48, pp. 125–129, 1989.
[17] L. Vicari, "Truncation of nondiffracting beams," *Optics Commun.*, vol. 70, no. 4, pp. 263–266, Mar. 15, 1989.
[18] M. Zahid and M. S. Zubairy, "Directionally of partially coherent Bessel-Gauss beams," *Optics Commun.*, vol. 70, no. 5, pp. 361–364, Apr. 1, 1989.
[19] S. Y. Cai, A. Bhattacharjee, and T. C. Marshall, " 'Diffraction-free' optical beams in inverse free electron laser acceleration," *Nuclear Instruments and Methods in Physics Research, Section A: Accelerators, Spectrometers, Detectors, and Associated Equipment*, vol. 272, no. 1–2, pp. 481–484, Oct., 1988.
[20] D. K. Hsu, F. J. Margetan, and D. O. Thompson, "Bessel beam ultrasonic transducer: fabrication method and experimental results," *Appl. Phys. Lett.*, vol. 55, no. 20, pp. 2066–2068, Nov. 13, 1989.
[21] J. Lu and J. F. Greenleaf, "Ultrasonic nondiffracting transducer for medical imaging," *IEEE Trans. Ultrason., Ferroelec., Freq. Contr.*, vol. 37, no. 5, pp. 438–447, Sept. 1990.
[22] ——, "Pulse-echo imaging using a nondiffracting beam transducer," *U.S. Med. Biol.*, vol. 17, no. 3, pp. 265–281, May 1991.
[23] ——, "Evaluation of a nondiffracting transducer for tissue characterization," in *Proc.1990 Ultrason. Symp.*, Honolulu, HI, 90CH2938–9, vol. 2, Dec. 4–7, 1990, pp. 795–798.
[24] ——, "A computational and experimental study of nondiffracting transducer for medical ultrasound," *Ultrason. Imag.*, vol. 12, no. 2, pp. 146–147, Apr. 1990. (abst)
[25] ——, "Simulation of imaging contrast of nondiffracting beam transducers", *J. Ultrasound Med.*, vol. 10, no. 3, (suppl), p. S4, Mar. 1991. (abst)
[26] J. A. Campbell and S. Soloway, "Generation of a nondiffracting beam with frequency independent beam width," *J. Acoust. Soc. Am.*, vol. 88, no. 5, pp. 2467–2477, Nov., 1990.
[27] J. H. Mcleod, "The Axicon: a new type of optical element," *J. Opt. Soc. Am.*, vol. 44, p. 592, 1954.
[28] S. Fujiwara, "Optical properties of conic surfaces. I. Reflecting Cone," *J. Opt. Soc. Am.*, vol. 52, pp. 287–292, 1962.
[29] C. B. Burckhardt, H. Hoffmann, and P. A. Grandchamp, "Ultrasound axicon: A device for focusing over a large depth," *J. Acoust. Soc. Am.*, vol. 54, no. 6, pp. 1628–1630, Dec., 1973.
[30] K. Yamada and H. Shimizu, "Conical and toroidal piezoelectric polymer transducers for long range focusing," *IEEE Trans. Sonics Ultrason.*, vol. SU-30, p. 215, 1983.
[31] M. S. Patterson and F. S. Foster, "Acoustic fields of conical radiators," *IEEE Trans. Sonics Ultrason.*, vol. SU-29, no. 2, pp. 83–92, Mar. 1982.
[32] D. R. Dietz, "Apodized conical focusing for ultrasound imaging," *IEEE Trans. Sonics Ultrason.*, SU-29, no. 3, pp. 128–138, May 1982.
[33] M. Moshfeghi, "Sidelobe suppression in annular array and axicon imaging systems," *J. Acoust. Soc. Am.*, vol. 83, no. 6, pp. 2202–2209, June 1988.
[34] Jian-yu Lu and J. F. Greenleaf, "Experimental verification of Nondiffracting X waves," *IEEE Trans. Ultrason. Ferroelec., Freq. Contr.*, submitted for publication.
[35] I. S. Gradshteyn and I. M. Ryzhik, *Table of Integrals, Series, and Products*, corrected and enlarged ed. New York: Academic, 1980, ch. 17.
[36] A. V. Oppenheim and R. W. Schafer, *Digital Signal Processing*. Englewood Cliffs, NJ: Prentice-Hall, Inc., 1975, ch. 5.
[37] R. Bracewell, *The Fourier Transform and its Applications*. New York: McGraw-Hill, 1965, chs. 4 and 6.
[38] J. W. Goodman, *Introduction to Fourier Optics*. New York: McGraw-Hill, 1968, chs. 2–4.
[39] T. K. Song and S. B. Park, "Analysis of broadband ultrasonic field response and its application to the design of focused annular array imaging systems," Ultrason. Technol. 1987, Toyohashi Int. Conf. Ultrason. Technol, Toyohashi, Japan, Edited by Kohji Toda, MYU Res., Tokyo, 1987.
[40] J. Lu and J. F. Greenleaf, "Nondiffracting electromagnetic X waves," *IEEE Trans. Antennas Propag.*, submitted for review.
[41] P. M. Moise and H. Feshbach, *Methods of Theoretical Physics*, Part I. New York: McGraw-Hill, 1953, chs. 4 and 7.

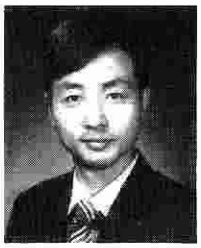

Jian-yu Lu (M'88) was born in Fuzhou, Fujian Province, People's Republic of China, on August 20, 1959. He received the B.S. degree in electrical engineering in 1982 from Fudan University, Shanghai, China, the M.S. degree in 1985 from Tongji University, Shanghai, China, and the Ph.D. degree in 1988 from Southeast University, Nanjing, China.

He is an Assistant Professor of Biophysics, Mayo Medical School, and a Research Associate, at the Biodynamics Research Unit, Department of Physiology and Biophysics, Mayo Clinic and Foundation, Rochester, MN. From 1988 to 1990, he was a postdoctoral Research Fellow there. Prior to that, he was a faculty member of the Department of Biomedical Engineering, Southeast University, and worked with Prof. Yu Wei. His research interests are in acoustical imaging and tissue characterization, medical ultrasonic transducers, and nondiffracting wave transmission.

Dr. Lu is a member of the IEEE UFFC Society, the American Institute of Ultrasound in Medicine, and Sigma Xi.

James F. Greenleaf (M'73–SM'84–F'88) was born in Salt Lake City, UT, on February 10, 1942. He received the B.S. degree in electrical engineering in 1964 from the University of Utah, Salt Lake City, the M.S. degree in engineering science in 1968 from Purdue University, Lafayette, IN, and the Ph.D. degree in engineering science from the Mayo Graduate School of Medicine, Rochester, MN, and Purdue University in 1970.

He is a Professor of Biophysics and Medicine, Mayo Medical School, and Consultant, Biodynamics Research Unit, Department of Physiology, Biophysics, and Cardiovascular Disease and Medicine, Mayo Foundation.

Dr. Greenleaf has served on the IEEE Technical Committee of the Ultrasonics Symposium since 1985. He served on the IEEE–UFFC Subcommittee for the Ultrasonics in Medicine/IEEE Measurement Guide Editors, and on the IEEE Medical Ultrasound Committee. He is Vice President of the UFFC Society. He holds five patents and is the recipient of the 1986 J. Holmes Pioneer award form the American Institute of Ultrasound in Medicine, and is a Fellow of the IEEE and the AIUM. He is the Distinguished Lecturer for the IEEE UFFC Society for 1990–1991. His special field of interest is in ultrasonic biomedical imaging science and has published more than 150 articles and edited four books.